This paper describes objective technical results and analysis. Any subjective views or opinions that might be expressed in the paper do not necessarily represent the views of the U.S. Department of Energy or the United States Government.

SAND2019-6253C

Bulk Power System Dynamics with Varying Levels of Synchronous Generators and Grid-Forming Power Inverters

Brian J. Pierre[1], Hugo N. Villegas Pico[2], Ryan T. Elliott[1], Jack Flicker[1], Yashen Lin[3], Brian B. Johnson[4], Joseph H. Eto[5], Robert H. Lasseter[6], and Abraham Ellis[1]

[1]Sandia National Laboratories, Albuquerque, NM, USA, [2]Iowa State University, Ames, IA, USA, [3]National Renewable Energy Laboratory, Golden, CO, USA, [4]University of Washington, Seattle, WA, USA, [5]Lawrence Berkeley National Laboratory, Berkeley, CA, USA, [6]University of Wisconsin-Madison, Madison, WI, USA

Abstract — **Inverters using phase-locked loops for control depend on voltages generated by synchronous machines to operate. This might be problematic if much of the conventional generation fleet is displaced by inverters. To solve this problem, grid-forming control for inverters has been proposed as being capable of autonomously regulating grid voltages and frequency. Presently, the performance of bulk power systems with massive penetration of grid-forming inverters has not been thoroughly studied as to elucidate benefits. Hence, this paper presents inverter models with two grid-forming strategies: virtual oscillator control and droop control. The two models are specifically developed to be used in positive-sequence simulation packages and have been implemented in PSLF. The implementations are used to study the performance of bulk power grids incorporating inverters with grid-forming capability. Specifically, simulations are conducted on a modified IEEE 39-bus test system and the microWECC test system with varying levels of synchronous and inverter-based generation. The dynamic performance of the tested systems with grid-forming inverters during contingency events is better than cases with only synchronous generation.**

Index Terms — **Droop control, virtual oscillator control, grid-forming inverters, frequency control, inverter control, photovoltaic inverters.**

I. Introduction

Inverters with grid-forming controls, or simply grid-forming inverters, adjust their voltage magnitude and phase according to measured terminal conditions, e.g., active and reactive currents. This mode of control is called *grid-forming* because it is capable of regulating voltage and frequency in a similar manner to synchronous generators. For example, during contingencies, grid-forming inverter-based generation can increase or decrease its power output almost instantaneously to balance loads, regulate local voltages, and contribute to frequency control.

Classic *grid-following* inverter control techniques rely on phase-locked loops (PLLs) as well as proportional-integral (PI) regulators. In contrast, their operation relies on the existence of a voltage reference waveform whose magnitude and frequency are regulated externally by synchronous machines. However, such conditions might not exist if synchronous machines are greatly displaced in the future. In such scenarios, high penetrations of inverter-based generation with grid-following controls might make the grid susceptible to weak dynamic voltages and/or poorly regulated system frequency [1].

Motivated by the aforementioned problems, grid-forming controls for power inverters have been devised so they can operate autonomously, i.e., without relying on synchronous generation [2]–[5]. In order to study the transition of today's power system to one that is highly inverter-based, the interoperability of grid-forming controls with existing synchronous machines must be assessed to detect potential compatibility problems [6]. To this end, this paper presents and implements two positive-sequence grid-forming control models of inverters for power system studies: virtual oscillator control and droop control [7]. Both can do the following: (i) autonomously generate terminal voltages cycling at a common synchronous speed, (ii) regulate system voltage magnitudes, and (iii) meet a power system demand in a shared manner.

The first positive sequence grid-forming model presented is a control strategy based on virtual oscillator control (VOC) [8]–[9]. The VOC implements, numerically, the dynamics of a class of nonlinear oscillators to generate nominal inverter voltages that cycle at a synchronous speed [8]. The second positive sequence grid-forming model presented is a control strategy based on droop control. The droop regulator, via software, mimics the dynamics of synchronous machines as well as their voltage and speed regulators, albeit disregarding rotor dynamics. For a pertinent explanation of the grid-forming droop control model, see [10]. Notably, the two grid-forming control strategies have similar steady state operation [9].

In this paper, the grid-forming strategies are modeled for positive-sequence simulations in Section II. In Section III, the two positive sequence grid-forming models are implemented in PSLF and compared to classic synchronous generation cases.

Manuscript received June 3, 2019. (Corresponding author: Brian J. Pierre, e-mail: bjpierr@sandia.gov.)

Sandia National Laboratories is a multimission laboratory managed and operated by National Technology and Engineering Solutions of Sandia, LLC, a wholly owned subsidiary of Honeywell International, Inc., for the U.S. Department of Energy's National Nuclear Security Administration under contract DE-NA0003525. The views expressed in the article do not necessarily represent the views of the U.S. Department of Energy or the United States Government.

This work was authored in part by the National Renewable Energy Laboratory, operated by Alliance for Sustainable Energy, LLC, for the U.S. Department of Energy (DOE) under Contract No. DE-AC36-08GO28308. Funding provided by DOE Office of Energy Efficiency and Renewable Energy Solar Energy Technologies Office under award number DE-EE0000-1583.

Two contingencies are analyzed under two test systems, the microWECC [11] and a modified IEEE 39-bus test system. Three cases are compared: a base system with 100% synchronous generation, and two 50% photovoltaic (PV) generation cases with VOC or droop control. Conclusions are in Section IV and indicate that for the systems studied, inverters with grid-forming control have better dynamic performance than 100% synchronous generation cases.

II. Modeling

A. Preliminaries

The rationale of a positive-sequence simulation model of an inverter-based power plant driven by a grid-forming (GFM) control strategy is illustrated in Fig. 1. There, the inverter with grid-forming control (e.g., VOC and droop) represents the aggregation of several inverters of relatively small apparent power capacity. For modeling simplicity, we assume that the dc-link voltage, V_{dc}, is sufficient at all times to generate any GFM commanded ac voltage and that the inverter is lossless. Another positive sequence modeling approach is shown in [12].

In the positive-sequence domain, the inverter can autonomously generate an abstract terminal voltage phasor $V\angle\delta$ (representative in time-domain of three-phase voltage waveforms), having phase angle δ and frequency, ω. It is assumed that the ac voltages $V\angle\delta$ commanded by the GFM control are replicated precisely at the terminals of the inverter. Inverter voltage saturation because of dc-link limitations and nonidealities are not considered in the model. In Fig. 1, the voltage magnitude V_∞ in per unit and angle δ_∞ in radians, model a synchronous power grid that is observed behind a transmission line, for example.

To generate $V\angle\delta$ cycling at ω, the GFM regulator (VOC or droop) relies on: (i) a voltage magnitude reference V_r, (ii) an active power reference P_r, and (iii) a current phasor $\tilde{I}_f$ that is measured at the terminals of the inverter. The current phasor $\tilde{I}_f$ is representative of three-phase sinusoidal currents cycling at the per-unit angular speed of an abstract center of inertia:

$$\omega_e = \frac{\sum_k \omega_k H_k}{\sum_k H_k} \tag{1}$$

where ω_k and H_k represent, respectively, the per unit speed and inertia of the k-th rotor ($k = 1, \ldots, K$) of a synchronous machine interconnected in a power system. As is typically done in the analysis of bulk power systems, we introduce the dynamics of an abstract center-of-inertia reference angle:

$$\frac{d}{dt}\theta_e = \omega_b \omega_e \tag{2}$$

with $\omega_b = 120\pi$ rad/s. The speed in (2) is instrumental in modeling relative angles synthesized by VOC and droop controls in positive-sequence simulation frameworks.

B. Virtual Oscillator Control Model

The averaged dynamics of a virtual oscillator for inverter control having speed vs. power droop characteristics are [9]:

$$\frac{d}{dt}\bar{V} = \frac{\sigma}{2C}\left(\bar{V} - \frac{1}{\kappa_v^2}\bar{V}^3\right) + \frac{\kappa_v\,\kappa_i}{2C\bar{V}}\bar{Q} \tag{3}$$

$$\frac{d}{dt}\bar{\theta} = \frac{1}{\sqrt{LC}} - \frac{\kappa_v\,\kappa_i}{2C\bar{V}^2}\bar{P} \tag{4}$$

Here, $\bar{V}$ models the line-to-neutral peak voltage amplitude of the oscillator whereas $\bar{\theta} \in [0,2\pi)$ captures the angle of the voltage waveform to be synthesized by the inverter. For example, the synthesized time-domain voltage at the inverter terminals for phase 'a' is $v_a(t) = \bar{V}(t)\cos\bar{\theta}(t)$. The variables $\bar{P}$ and $\bar{Q}$ in (3) and (4) model average active and reactive power of a three-phase system, respectively. The constants σ, C, L, κ_v, κ_i are parameters that define the behavior of the virtual oscillator—for their significance and selection, please refer to [9].

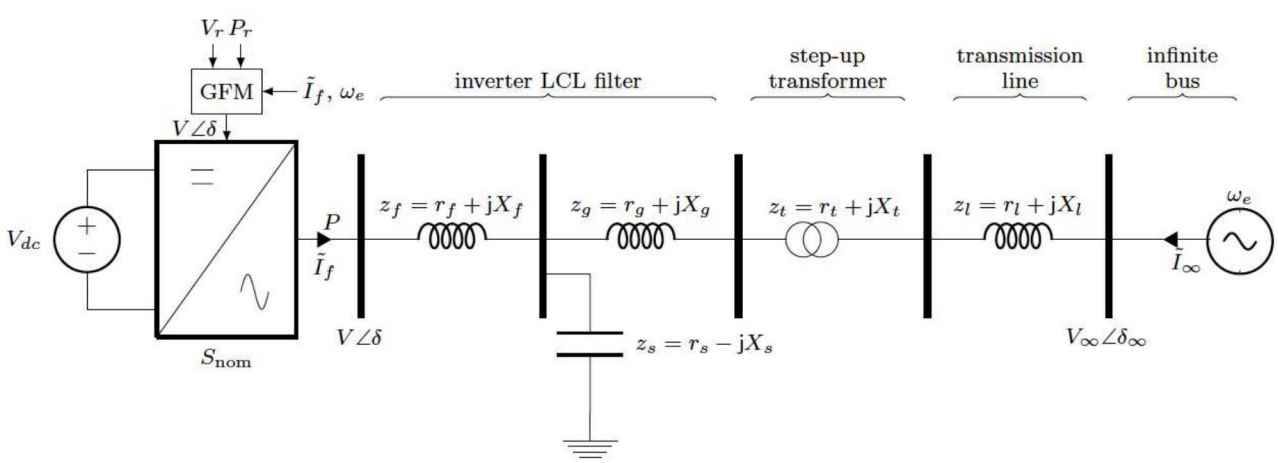

Fig. 1. Inverter-based power plant controlled with grid-forming controls and interconnected a bulk power system.

A per-unit representation of (3)–(4) is:

$$\frac{d}{dt}V = \frac{\sigma}{2C}V(1-V^2) - \frac{\kappa_i S_b}{2C}\frac{Q}{V} \tag{5}$$

$$\frac{d}{dt}\delta = \omega_b(\omega - \omega_e), \tag{6}$$

where

$$\omega = 1 - \frac{\kappa_i S_b}{2\omega_b C V_b}\frac{P}{V^2}. \tag{7}$$

The model (5)–(7) is from (3)–(4) by: (i) defining $\bar{V} = VV_b$, $\bar{P} = PS_b$, $\bar{Q} = QS_b$, and $d\bar{\theta}/dt = \omega\omega_b$ ($\omega_b = 1/\sqrt{LC}$) as well as (ii) referring $\bar{\theta}$ of (4) with respect to θ_e of (2), hence, $d\delta/dt = d\bar{\theta}/dt - d\theta_e/dt$. We consider a relative angle δ to avoid simulating cycling signals in the positive-sequence domain. We clarify that the field implementation of the VOC control does not rely on measuring θ_e of (2). The introduced constants V_b, S_b, and ω_b are peak line-to-neutral voltage base, three-phase voltampere base, and angular frequency base, respectively.

For grid-operation, the equilibrium points of (5)–(6) can be shifted by adding appropriate voltage and active power reference set-points, e.g., V_r and P_r. Also, by considering a dq-axis reference frame whose angle is, e.g., $\bar{\theta}$ from (4), the per-unit active and reactive power at the terminals of the inverter can be calculated via $P = Vi_{df}$ and $Q = -Vi_{qf}$ where $i_{df} + ji_{df} = e^{-j\delta}\tilde{I}_f$ (here, $j = \sqrt{-1}$ and e is the Euler's number). The latter phasor relationship results from a particular choice of reference-frame transformation form [13]. Using the aforementioned considerations, a per-unit positive-sequence dynamic model of an inverter representative of a power plant that is driven by VOC control is:

$$\frac{d}{dt}V = \frac{1}{2\tau_V}V(V_r^2 - V^2) - \kappa_q\frac{Q}{V} \tag{8}$$

$$\frac{d}{dt}\delta = \omega_b(\omega - \omega_e) \tag{9}$$

$$\omega = 1 - \frac{\kappa_P}{V^2}(P - P_r) \tag{10}$$

$$P = V\,i_{df} \tag{11}$$

$$i_{df} + ji_{qf} = e^{-j\delta}\tilde{I}_f \tag{12}$$

$$Q = -V\,i_{qf}. \tag{13}$$

The constants τ_V, κ_q and κ_p of (8) and (10) can be deduced from (5) and (7).

C. Droop Control Model

A per-unit positive-sequence dynamic model of an inverter with droop control is:

$$\frac{d}{dt}V = \frac{1}{\tau_V}\left(V_r - V - \kappa_Q Q\right) \tag{14}$$

$$\frac{d}{dt}\delta = \omega_b(\omega - \omega_e). \tag{15}$$

The linear dynamics of (3) and (4) represent the voltage and relative angle synthesized by the droop controller. In particular, the dynamics of (4) are obtained by referencing the droop controller angle dynamics $d\theta/dt = \omega_b\omega$ to $d\theta_e/dt$ of (2) where

$$\omega = 1 - \kappa_P(P - P_r) \tag{16}$$

is the cycling speed of the synthesized voltages by the droop control, which depends on measured active power P as well as its set point P_r. The reactive, Q, and active, P, powers for (14) and (16) are obtained dynamically via the first-order filters

$$\frac{d}{dt}Q = \frac{1}{\tau_S}\left(-Q - V\,i_{qf}\right) \tag{17}$$

$$\frac{d}{dt}P = \frac{1}{\tau_S}\left(-P + V\,i_{df}\right) \tag{18}$$

which filter negative-sequence components. Here, i_{df} and i_{qf} are inverter currents in the droop-controller reference frame and are calculated as follows $i_{df} + ji_{qf} = e^{-j\delta}\tilde{I}_f$. Overall, the droop model, defined by (14)–(18), has significant resemblance to the VOC model defined by (8)–(13), albeit originating from different technologies. Specifically, the voltage dynamics of (3) and (4) derive from a Van der Pol oscillator expressed in polar coordinates after averaging. Notably, negative-sequence filters for reactive and active power, i.e., (17)–(18), are not necessary in the VOC model because the controlled implementation of the controller relies on waveform-level current measurements [8]–[9].

D. Initialization of Grid-Forming Controls

To initialize the VOC control, we assume that the voltage magnitude, $V(0) = V_0$, and active power, $P(0) = P_0$, generated by the grid-forming inverter at its terminals are known at the pre-transient state, i.e., at $t = 0$. In other words, assume that the terminals of the aggregated inverter representation of Fig. 1 are abstracted as a 'PV' bus as is classically done in the analysis of synchronous generation [14]. To obtain the abstracted inverter terminal current phasor, $\tilde{I}_f(0) = \tilde{I}_{f0}$, and voltage angle, $\delta(0) = \delta_0$, the classical numerical approach to solve the power flow problem is assumed to be applied [14]. Note here that the power flow solution will depend on the types of generating sources and load assets that are connected to a particular power system.

Hence, the initial VOC control states for (8) and (9) are $V(0) = V_0$ and $\delta(0) = \delta_0$, respectively. The set-points, on the other hand, are obtained as follows:

a) calculate $i_{df} + ji_{qf} = e^{-j\delta_0}\tilde{I}_{f0}$,
b) calculate $V_r > 0$ from (9) because at pre-transient: $\frac{d}{dt}V_0 = 0 = \frac{1}{2\tau_V}V_0\left(V_r^2 - {V_0}^2\right) + \kappa_q\,i_{qf}$, and
c) assign $P_r = P_0$, hence $\omega(0) = 1$ p.u. of ω_b.

Initialization of the droop-based grid-forming inverter control model is similar to the VOC case and hence not discussed.

III. Comparison of Grid-forming Inverters and Synchronous Generators in Bulk Power Systems

The two models are specified for use in positive-sequence simulation frameworks. Both the VOC and droop models are, in a way, trying to mimic control and dynamic performance of traditional synchronous generation. The VOC and droop model parameters are set to have similar frequency-droop (5%) and voltage-droop (2%) characteristics as the synchronous generation in the two test systems. Reference [15] discusses the placement and simulates grid-forming and grid-following inverter models.

The models are compared during a load trip event on a modified IEEE 39-bus test system. The IEEE 39-bus test system is a well-known system that represents a part of the U.S. eastern interconnection. In addition, the models are compared during a generation trip event on a modified microWECC [11] test system, which is a scaled down version of the North American Western Interconnection in Fig. 2. The microWECC system was developed at Montana Tech, and is primarily used here because it allows analysis on a system prone to a large frequency nadir and oscillations (compared to the IEEE 39-bus system).

Three cases are compared: 100% synchronous generator case, ~50% PV case with VOC grid-forming inverter model, ~50% PV case with grid-forming droop model. The original IEEE 39-bus test system and the microWECC were modified to include:

a. governor models with 5% droop on all synchronous generators,
b. custom data recording model to help with post analysis processing,
c. the custom grid-forming PV inverter models,
d. modern exciter models with 2% voltage droop,
e. and on the IEEE 39-bus test system, the load models were updated to a more modern load model, (20% motor load, 20% constant impedance load, 60% constant power load).

To construct the PV cases, each original synchronous generator in the test systems is split into an inverter-based generator and a synchronous generator on parallel buses. In all cases, it is assumed that sufficient headroom exists on the PV bus to inject power into the system in case of a contingency (e.g., solar is curtailed when connected to the transmission grid).

Multiple contingencies were simulated to determine the performance of the grid-forming inverter models; two are shown in this paper. First, a load trip event on the IEEE 39-bus test system, and second, a generation trip event on the microWECC system.

A. Load Trip Event on the IEEE 39-bus system

The first contingency simulated on the IEEE 39-bus test system is a load trip of 158 MW (2.59% of the system) and 30 MVAr (2.13% of the system). The weighted system frequency (system frequency at all generator buses, weighted by power output of the generators) is shown in Fig. 3. The settling frequency of the 50% PV cases is effectively the same as in the 100% synchronous case. This indicates that the droop characteristic programmed into the inverter-based generation controls matches the setting of the synchronous generator turbine governors. The settling frequency in the VOC case deviates slightly from the other two because its dynamics do not precisely correspond to a linear droop characteristic [8].

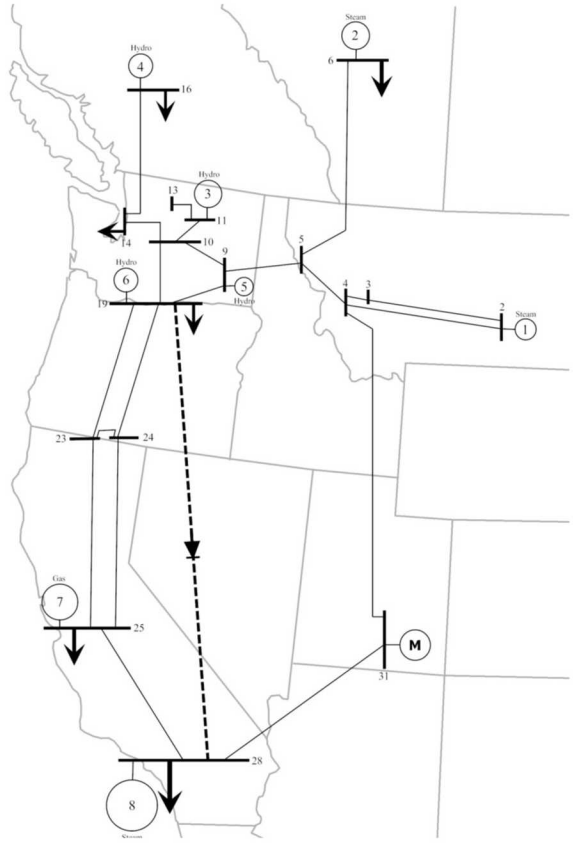

Fig. 2. The microWECC test system [11].

The output power of a synchronous machine and the parallel PV generator during the contingency is shown in Fig. 4 and Fig. 5, respectively. The change in active power shown in Fig. 4 varies between the 100% synchronous case and the 50% PV cases because the capacity of the synchronous generator is scaled down when the inverter-based generation is introduced. In each case, the change in output power of the synchronous machine matches the anticipated turbine governor response. Note that the 100% synchronous generation case in Fig. 4 contains an offset to account for differences in the dispatch pattern between the cases with and without PV.

Fig. 6 shows the voltage transient at the same synchronous generator bus as in Fig. 4. This plot effectively compares the voltage regulation achieved purely using the automatic voltage regulator (AVR) and excitation system of the synchronous machine with that achieved by the combined efforts of the syn-

chronous and inverter-based generator controls. The results indicate similar transients in all three cases, with perhaps slightly better damping in the 50% PV cases. These differences are sensitive to whether a power system stabilizer (PSS) is modeled and the precise details of its implementation. The voltage regulation characteristics of the VOC and droop-based controls are substantially similar.

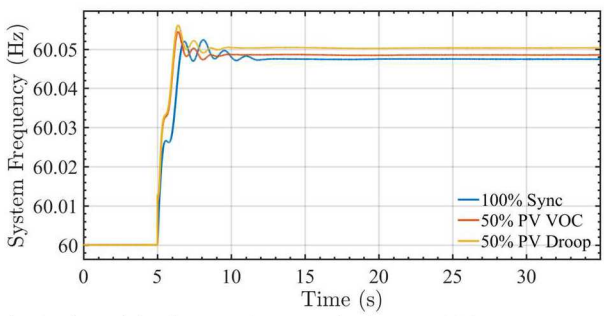

Fig. 3. The weighted system frequency in the IEEE 39-bus test system during a load trip.

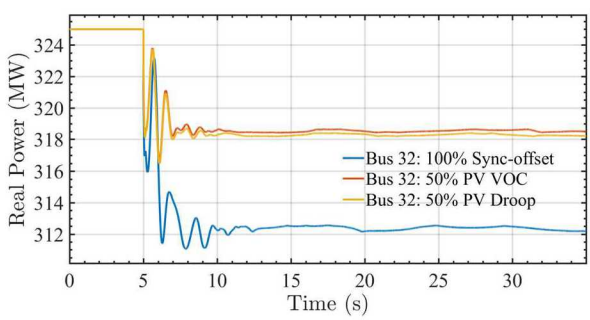

Fig. 4. The output power of a synchronous generator in the IEEE 39-bus test system during a load trip.

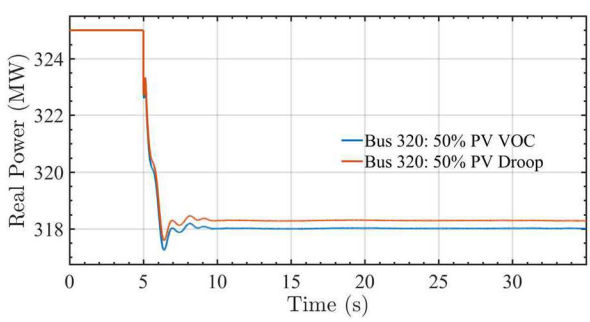

Fig. 5. The output power of a PV generator in the IEEE 39-bus test system during a load trip.

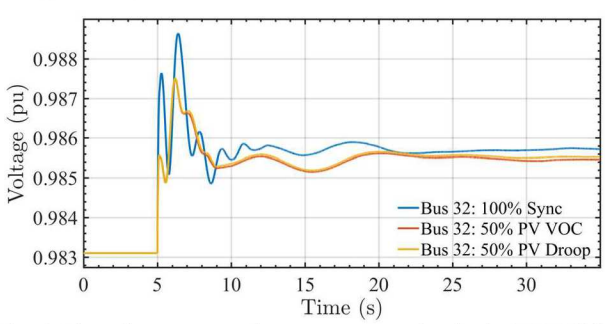

Fig. 6. The voltage at a synchronous generator bus in the IEEE 39-bus test system during a load trip.

B. Generation Trip Event on the MicroWECC

The second contingency simulated on the microWECC system is a generation trip event of a synchronous machine in the northwest (in Fig. 2) with an MVA base of 9000, and at the time of the trip, producing 1256 MW (2.58% of the system). Fig. 7 shows the trajectory of the system frequency in response to the contingency. The microWECC system was employed for this analysis because it demonstrates a deeper frequency nadir than the IEEE 39-bus system model. Fig. 7 shows that the cases with 50% PV exhibit significantly less overshoot in the step response than the 100% synchronous case. This indicates that the addition of the inverter-based controls has a stabilizing effect on the frequency regulation mode, the lowest natural resonant frequency of the system. As observed following the generation trip, the settling frequency of the 50% PV cases matches that of the 100% synchronous case almost exactly.

Fig. 8 shows the real power output for the synchronous generator at bus 1. The traces for the VOC and droop cases effectively lie on top of one another. As in Fig. 4, the change in power varies between the cases with and without PV because the capacity of the synchronous generator is adjusted when the inverter-based generation is introduced. The cases with inverter-based generation controls exhibit markedly better damping than the 100% synchronous case for this contingency. As in Fig. 4, the 100% synchronous generation case in Fig. 8 contains an offset to account for differences in the dispatch pattern between the cases with and without PV. Fig. 9 shows the corresponding change in real power output for the parallel PV generator at bus 1.

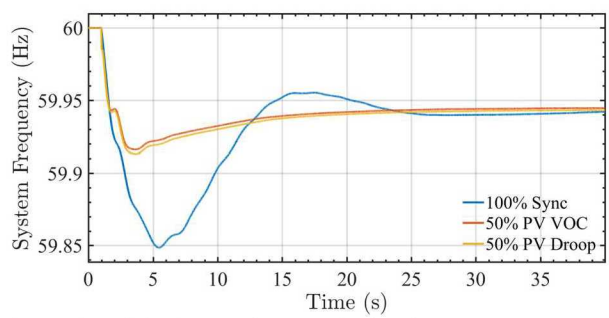

Fig. 7. The weighted system frequency in the microWECC test system during a generation trip.

Fig. 10 shows the voltage transient at bus 1 during the generation trip event. The results indicate better overall performance in the 50% PV cases with significantly improved oscillation damping. As in the first contingency, the differences between the cases with and without PV shown in Figs. 7-10 are sensitive to whether PSSs are modeled and how they are implemented. In the microWECC test system only two synchronous generators include PSSs.

The primary takeaway from analyzing these contingencies is that grid-forming inverter controls are capable of supplementing and/or replacing the governor response, voltage support, and oscillation damping traditionally provided by synchronous machines.

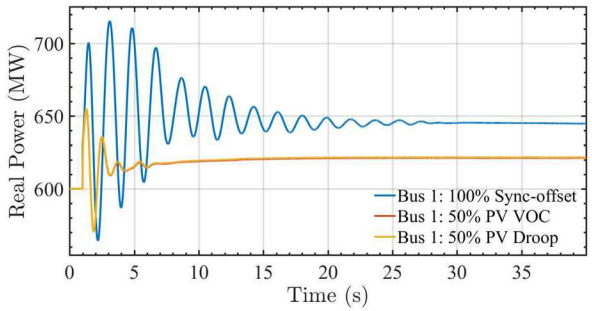

Fig. 8. The output power of a synchronous generator in the microWECC test system during a generation trip.

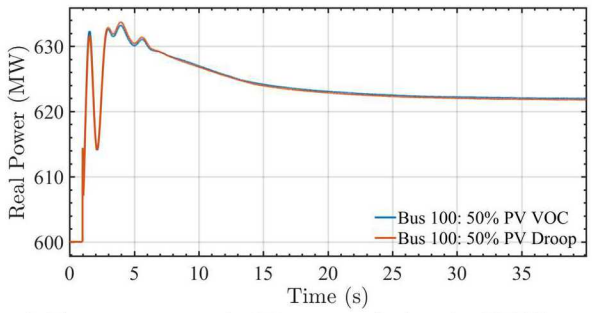

Fig. 9. The output power of a PV generator in the microWECC test system during a generation trip.

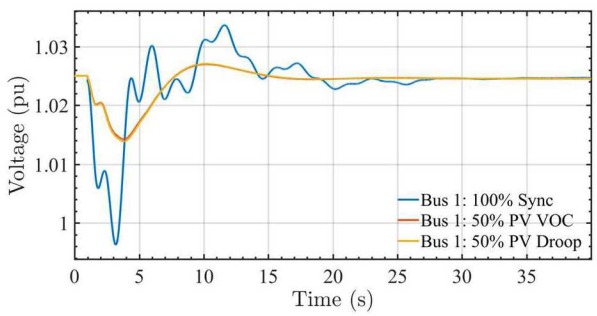

Fig. 10. The voltage at a synchronous generator bus in the microWECC test system during a generation trip.

IV. Conclusion

This paper presents two positive-sequence grid-forming inverter control models and compares the models in bulk power system simulations. Custom dynamic models were developed in PSLF for the two grid-forming inverter controls algorithms. Generation and load trip events were simulated for a modified microWECC test system and IEEE 39-bus test system respectively for three cases: 100% synchronous generation, ~50% PV penetration with the virtual oscillator control grid-forming inverter model, and ~50% PV penetration case with a droop-based grid-forming inverter control model. The results from these simulations indicate that under typical contingencies, the grid-forming inverter models can have similar or better dynamic performance to traditional 100% synchronous generation if the parameters of the control schemes are chosen appropriately. The results are promising, but future work needs to continue research in this area, especially in fault analysis and protection for grid-forming inverters.

The considered models are primarily intended to be applied in contingency analyses that are typically conducted during power system planning studies. For now, the presented models are not suitable to study the fault ride-through capability of inverter-based resources because this functionality has not been added thus far. Incorporating such capability is possible by, for example, switching the inverter control strategy from voltage to current regulation during faults. However, the impact that this or other possible approaches have on the power-system level performance is under investigation.

Another limitation of the presented models is that they do not incorporate the primary energy sources, e.g., wind and photovoltaic solar. Nonetheless, these could be integrated by considering the dc-link dynamics in the representations, e.g., see [13].

References

[1] N. Miller, B. Leonardi, R. D'Aquila, K. Clark, "Western wind and solar integration study phase 3A: Low levels of synchronous generation," National Renewable Energy Laboratory Technical Report TP-5D00-64822, 2015.

[2] M. Chandorkar, D. M. Divan, and R. Adapa, "Control of parallel connected inverters in standalone ac supply systems," *IEEE Trans. Ind. Appl.*, vol. 29, pp 136–143, Jan./Feb. 1993.

[3] R. Lasseter and P. Piagi, "Providing premium power through distributed resources," presented at *33rd Hawaii Int. Conf. Syst. Sciences*, Maui, HI, Jan. 7, 2000.

[4] J. M. Guerrero, M. Chandorkar, T-L Lee, and P. C Loh, "Advanced control architectures for intelligent microgrids—Part I: Decentralized and hierarchical control," *IEEE Trans. Ind. Electron.*, vol. 60, no. 4, Apr. 2013.

[5] J. Schiffer, R. Ortega, A. Astolfi, J. Raisch, and T. Sezi, "Conditions for stability of droop-controlled inverter-based microgrids," *Automatica*, vol. 50, no. 10, pp. 2457–2469, Oct. 2014.

[6] J. Schiffer, D. Golding, J. Raisch, and T. Sezi, "Synchronization of droop-controlled microgrids with distributed rotational and electronic generation," presented at *52nd IEEE Conf. Decision and Control*, Florence, Italy, Dec. 10–13, 2013.

[7] H. N. Villegas Pico, Y. Lin, B. Johnson, "Positive-sequence inverter models with controllers based on virtual oscillator, speed droop, and phase-locked loop," National Renewable Energy Laboratory, Tech. Rep. in press.

[8] B. Johnson, S. Dhople, A. Hamadeh, and P. Krein, "Synchronization of parallel single-phase inverters with virtual oscillator control," *IEEE Trans. Power Electronics*, vol. 29, pp. 6124–6138, Nov. 2014.

[9] B. Johnson, M. Rodriguez, M. Sinha, and S. Dhople, "Comparison of virtual oscillator and droop control," presented at *IEEE 18th Workshop on Control and Modeling for Power Electronics* (COMPEL), July 2017.

[10] W. Du, Q. Jiang, M. Erickson, R. Lasseter, "Voltage-source control of PV inverter in CERTS microgrid," *IEEE Trans. Power Del.*, vol. 29, no. 4, Aug. 2014.

[11] R. Hallett, "Improving a transient stability control scheme with wide-area synchrophasors and the microWECC, a reduced-order model of the western interconnect," M.S. Thesis, Electrical Engineering Department, Montana Tech, Butte, MT, USA, 2018.

[12] D. Ramasubramanian, Z. Yu, R. Ayyanar, V. Vittal and J. Undrill, "Converter Model for Representing Converter Interfaced Generation in Large Scale Grid Simulations," *IEEE Trans. Power Syst.*, vol. 32, no. 1, pp. 765-773, Jan. 2017.

[13] H. N. Villegas Pico and B. B. Johnson, "Transient stability assessment of multi-machine multi-converter power systems," *IEEE Trans. Power Syst.*, accepted for publication.

[14] Wood, A. J., and B. F. Wollenberg. 1996. Power Generation, Operation, and Control. 2nd ed. New York: John Wiley & Sons.

[15] B. K. Poolla, D. Gross, and F. Dörfler. "Placement and Implementation of Grid-Forming and Grid-Following Virtual Inertia and Fast Frequency Response," *IEEE Trans. Power Syst.*, Jul. 2018.